NUMERICAL STUDY OF FLOW AND HEAT TRANSFER IN A POROUS MEDIUM BETWEEN TWO STRETCHABLE DISKS USING QUASI-LINEARIZATION METHOD

Shaheen AKHTER [1,2], Muhammad ASHRAF [2,*]

[1] Departement of Mathematics, COMSATS University Islamabad, Sahiwal-Campus, Pakistan

[*2] Centre for Advanced Studies in Pure and Applied Mathematics (CASPAM), Bahauddin Zakariya University Multan, Pakistan.

[*] Corresponding author; E-mail: *muhammadashraf*@bzu.edu.pk

2. *akhter_math*@yahoo.com

In this study, the flow as well as heat transfer of a classical Newtonian fluid of constant density and viscosity in a porous medium between two radially stretching disks is explored. The role of the porosity of the medium, the stretching of the disks, the viscous dissipation and radiation on the flow and temperature fields is taken into account. The flow and heat equations are transformed into nonlinear ordinary differential equations by invoking the classical similarity transformations. These nonlinear differential equations were linearized using Quasi linearization method. Further the linearized equations were discretized by employing the finite differences which were then solved numerically using the successive over relaxation parameter method. Some features of the flow and temperature are discussed in detail in the form of tables and graphs. The present study may be beneficial in lubricants and computational storage devices as well as fluid flows and heat transmission in rotor-stator systems.

Key words*: stretchable disks, porous medium, heat transfer, viscous dissipation, Quasi-linearization*

1. Introduction

The applications involving flow between two disks are in mass exchangers, heat control, rotating machineries, crystal growth processes, lubricants and computational storage devices. The disks are separated with the help of lubricant vaccinated into them. In addition to that, polymer additive fluids are used as enhanced lubricating oils in current lubrication technologies. The porous medium bounded by heated or cooled surface is used to inject fluid that is being adopted in many application areas including control of boundary layer, film cooling *etc*. Similarly, fluid flows and heat transmitted in rotor-stator systems have greater usability in turbo machinery and power engineering domain.

At low Reynolds number, for the simulation of fluid flow, Darcy's law is much appropriate. Masoud *et al.* [1] investigated experimentally the effect of permeability and inertial forces over a fluid flow through a porous medium. They also studied the derivations of Navier Stokes equations and coefficient of inertial term experimentally as well as numerically by using Darcy Law.

Numerical solution had been done based on the boundary elements method. For flows with higher Reynolds number, the Forchheimer term coefficients could be obtained from experimental investigations. The problem of a Newtonian fluid flow through microfabricated hyperbolic contractions was studied numerically using finite volume method in detail by Mónica *et al.* [2]. Experimentally, they investigated the kinematics in contraction region by way of micro particle image velocimetry. From this technique they were able to characterize the velocity field quantitatively in the hyperbolic contraction region at a given plane. Hamza [3] presented numerically the similarity solution of fluid flow between two parallel disks in the presence of perpendicularly applied magnetic field. Analytical solution of steady incompressible flow between two uniformly co-rotating disks was discussed by Milan [4] and results were compared by numerical solution. The rheological properties of Newtonian and non-Newtonian fluids are widely measured by viscometer. Yeow *et al.* [5] presented the numerical solution of viscous steady Newtonian fluid flow through parallel viscometer disks using separation of variable method. They concluded that under wall slip, the azimuthal velocity varied linearly for a short time in the radial direction. Lynn *et al.* [6] provided the numerical solution of the viscous fluid flow between two coaxial infinite disks, keeping one disk stationary and the other one rotating. They also discussed the uniform suction effects through the rotating disk. Hydrodynamic behavior of two fluids at low Reynolds number, both having different density and viscosity between a rotating and a stationary disk was explored by Zweig *et al.* [7]. Qayyum *et al.* [8] discussed the problem of non-steady axisymmetric Jeffrey fluid flow between two parallel disks. Jain *et al.* [9] numerically investigated the effect of radiation on fluid flow in a porous medium over a rotating permeable disk. They analyzed the effects of different parameters like Prandtl number, Knudsen number, rotational Reynolds number, porosity parameter and temperature on velocity and temperature distributions by keeping the fluid properties constant as well as temperature dependent and depicted results through tables and graphs. By using the method of Lattice Boltzmann, Wijaya *et al.* [10] presented the numerical simulation of problem fluid flow and heat transfer in porous medium like geothermal reservoir. Hussain [11] discussed the nano fluids with convection of mass and heat transfer of non-compressible viscous fluid through porous disks using SOR method. Numerically investigation of the effects of thermal radiation and viscous dissipation through porous medium over a non-linearly stretched sheet was discussed by Nandeppanavar *et al.* [12]. Srinivasacharya *et al.* [13] studied the radiation effects and chemical reactions in a porous medium with convection mass and heat transfer over a vertical plate set in a power-law fluid numerically. The similarity solution of unsteady laminar flow of a viscous incompressible fluid over a stretching rotating disk was investigated analytically and numerically by Hobiny *et al.* [14]. Analytical results were compared by numerical results. Sreenivasulu *et al.* [15] presented the effects of thermal radiation and viscous dissipation on MHD boundary layer flow over a permeable stretching surface. Rashidi *et al.* [16] used the homotopy analysis method to provide the numerical solution of fluid flow with heat transfer analysis over the rotating disk in a porous medium. Raja *et al.* [17] investigated numerically the effects of entropy generation and thermal effects with no slip conditions in porous microducts by using Boltzmann method. Analytical solution for the problem of asymmetrical heating effects in an annular porous medium was given by Huijin *et al.* [18]. Turkyilmazoglu [19] presented the exact solution of Navier-Stokes equations in cylindrical coordinates system and investigated numerically the solution of the problem of fluid flow and heat transfer analysis between two stretchable rotating disks.

We want to analyze the flow and heat transfer of an incompressible viscous fluid through a resistive porous medium between two stretchable infinite disks numerically using Quasi linearization method taking into consideration the effects of viscous dissipation and radiation.

2. Mathematical analysis

Consider the steady flow along with heat transfer and radiation of a fluid of constant density and viscosity between stretchable disks. The porous medium between the disks resists the fluid motion. The lower disk is situated at the infinite horizontal plane $z = -h$ whereas the upper one is

located at $z = h$ as seen in Fig. 1. For the study of disk flow problem, it is convenient to use the cylindrical polar coordinate system. Both the disks are linearly stretched in the radial direction. The flow velocity field $\vec{v} = (u, v, w)$ can be written, mathematically, as

$$u = u(\mathrm{r},\mathrm{z}), \quad v = 0, \quad w = w(\mathrm{r},\mathrm{z}), \tag{1}$$

where $u, v \,\&\, w$ are respective velocity components in the radial, transverse and axial directions. Keeping in view the flow assumptions and following the Eringen's work [20, 21] the governing equations for flow through a resistive porous medium between two disks may be summarized as

$$\frac{u}{r} + \frac{\partial u}{\partial r} + \frac{1}{h}\frac{\partial w}{\partial \eta} = 0, \tag{2}$$

$$\rho\left(u\frac{\partial u}{\partial r} + \frac{w}{h}\frac{\partial u}{\partial \eta}\right) = -\frac{\partial p}{\partial r} + \mu\left(\frac{\partial^2 u}{\partial r^2} + \frac{1}{r}\frac{\partial u}{\partial r} - \frac{u}{r^2} + \frac{1}{h^2}\frac{\partial^2 u}{\partial \eta^2}\right) - \frac{\mu}{\kappa^{\bullet}}u, \tag{3}$$

$$\rho\left(u\frac{\partial w}{\partial r} + \frac{w}{h}\frac{\partial w}{\partial \eta}\right) = -\frac{1}{h}\frac{\partial p}{\partial \eta} + \mu\left(\frac{\partial^2 w}{\partial r^2} + \frac{1}{r}\frac{\partial w}{\partial r} + \frac{1}{h^2}\frac{\partial^2 w}{\partial \eta^2}\right) - \frac{\mu}{\kappa^{\bullet}}w, \tag{4}$$

in these equations, μ is the dynamic viscosity, η is the similarity variable, p is the pressure, $k^{\bullet}$ is the Darcy permeability and ρ is the density of the fluid. In order to study the thermal characteristics of the flow through the resistive medium between the disks, the energy equation including the radiation & viscous dissipation terms, may be expressed as

$$\rho c_p\left(v\frac{\partial T}{\partial r} + \frac{u}{h}\frac{\partial T}{\partial \eta}\right) = k_{\circ}\left(\frac{1}{h^2}\frac{\partial^2 T}{\partial \eta^2} + \frac{\partial^2 T}{\partial r^2} + \frac{1}{r}\frac{\partial T}{\partial r}\right) - \frac{1}{h}\frac{\partial q_r}{\partial \eta} + \frac{\mu}{h^2}\left(\frac{\partial v}{\partial \eta}\right)^2, \tag{5}$$

where c_p, T and $k_{\circ}$ are the specific heat capacity, the temperature and the thermal conductivity of the fluid respectively.

The radiative heat flux q_r may be defined as

$$q_r = -\frac{4\sigma}{3k^* h}\frac{\partial T^4}{\partial \eta}, \tag{6}$$

where σ is the Stefan-Boltzmann constant and k^* is the mean absorption coefficient. For the small temperature differences within the flow field, the term T^4 may be linearized. Thus, T^4 is expanded about T_{∞} by Taylor series approximation and by neglecting the terms of higher order as

$$T^4 \cong 4T_{\infty}^3 T - 3T_{\infty}^4. \tag{7}$$

Using this approximation in Eq. (5), we get

$$\rho c_p\left(u\frac{\partial T}{\partial r} + \frac{w}{h}\frac{\partial T}{\partial \eta}\right) - k_{\circ}\left(\frac{1}{h^2}\frac{\partial^2 T}{\partial \eta^2} + \frac{\partial^2 T}{\partial r^2} + \frac{1}{r}\frac{\partial T}{\partial r}\right) - \frac{16\sigma T_{\infty}^3}{3k^* h^2}\frac{\partial^2 T}{\partial \eta^2} - \frac{\mu}{h^2}\left(\frac{\partial u}{\partial \eta}\right)^2 = 0. \tag{8}$$

Boundary conditions for the flow velocity and temperature distribution at the lower as well as the upper disk are given as,

$$u(r,-h) = rS_1,\ u(r,h) = rS_2,\ w(r,-h) = 0,\ w(r,h) = 0,\ T(r,-h) = T_1,\ T(r,h) = T_2, \tag{9}$$

where $S_2 \,\&\, S_1$ (both having units of $[t^{-1}]$) are the stretching strengths of the upper and lower disks respectively. First two boundary conditions in equation (9) are due to the radial stretching of the disks. Since the disks are non porous so the axial velocity $w(r,z)$ at the lower and upper disks is zero. The two disks are kept at constant temperature $T_1 \,\&\, T_2$ respectively. By using the similarity variables, the Partial differential Equations (3) - (4) and (8) are transformed into ordinary ones

$$\eta = \frac{z}{h}, \quad u = -\frac{rS_1}{2}g'(\eta), \quad w = S_1 h g(\eta), \quad \theta(\eta) = \frac{T - T_2}{T_1 - T_2}. \tag{10}$$

The expressions for dimensionless velocities g and g' may be obtained from the continuity and momentum equations and the stream function by comparing the order of the terms. Velocity field (given in Eq. (10)), shows a possible fluid motion as it satisfies the continuity equation (1). Equations (3)–(4) & (8), in view of Eq. (10), reduce to

$$g''' - R_e g g''' - \varepsilon g'' = 0, \tag{11}$$

$$\left(1+\frac{4}{3}Rd\right)\theta''-R_e\,\mathrm{Pr}\,g\theta'+\frac{1}{4}\mathrm{Pr}\,E_n g''^2=0, \tag{12}$$

where prime denotes the derivative w.r.t involved variable η, $\mathrm{R}_e=\dfrac{\rho S_1 h^2}{\mu}$ is the stretching Reynolds number, $E_n=\dfrac{r^2 {S_1}^2}{\left[c_p\left(T_1-T_2\right)\right]}$ is the Eckert number, $\mathrm{Pr}=\dfrac{\mu c_p}{k_\circ}$ is the Prandtl number, $Rd=\dfrac{4\sigma T_\infty^3}{k^* k_\circ}$ is the radiation parameter and $\varepsilon=\dfrac{h^2}{k^\bullet}$ is the porosity parameter. The expression for g'' at the boundary is determined by using Newton's law of viscosity.

The conditions given in equation (9) become,

$$g(-1)=g(1)=0,\quad g'(-1)=-2,\quad g'(1)=-2\alpha,\quad \theta(-1)=1,\quad \theta(1)=0. \tag{13}$$

Here $\alpha=S_2/S_1$ is the relative disk stretching parameter.

3. Computational procedure

The method of Quasi-linearization is useful to convert the higher order nonlinear equations into linear form. By using this method the numerical solution is obtained as follows:

We construct the vector sequences $\left\{g^{(k)}\right\}$ and $\left\{\theta^{(k)}\right\}$. These converge to the respective numerical solution of Eqs. (11) and (12). We linearize Eq. (11) by retaining only the first order terms to construct $\left\{g^{(k)}\right\}$. For this purpose, we set

$$L\left(g,g',g'',g''',g'''\right)=g'''-R_e g g'''-\varepsilon g'',$$

which gives rise to:

$$L\left(g^{(k)},g'^{(k)},g''^{(k)},g'''^{(k)},g'''^{(k)}\right)+\left(g^{(k+1)}-g^{(k)}\right)\frac{\partial L}{\partial g^{(k)}}+\left(g'^{(k+1)}-g'^{(k)}\right)\frac{\partial L}{\partial g'^{(k)}}$$

$$+\left(g''^{(k+1)}-g''^{(k)}\right)\frac{\partial L}{\partial g''^{(k)}}+\left(g'''^{(k+1)}-g'''^{(k)}\right)\frac{\partial L}{\partial g'''^{(k)}}+\left(g'''^{(k+1)}-g'''^{(k)}\right)\frac{\partial L}{\partial g'''^{(k)}}=0.$$

After simplification, we get

$$g'''^{(k+1)}-R_e g^{(k)} g'''^{(k+1)}-\varepsilon g''^{(k+1)}-R_e g^{(k+1)} g'''^{(k)}=-g^{(k)} g'''^{(k)} R_e. \tag{14}$$

Eq. (14) provides the system of the ODEs. Here, $g^{(k)}$ represents the solution vector of the k^{th} equation. For solving the linear equations, the derivatives are replaced by employing the central difference approximations. It gives rise to the sequence $\left\{g^{(k)}\right\}$, generated by the following linear system

$$Gg^{(k+1)}=H \text{ with } G\equiv G_{n\times n}\left(g^{(k)}\right) \text{ and } H\equiv H_{n\times 1}\left(g^{(k)}\right), \tag{15}$$

where the total number of grid points is represented by n. Since the Eq. (12) is linear in θ, so to generate the sequence $\left\{\theta^{(k)}\right\}$, we may write,

$$\left(1+\frac{4}{3}Rd\right)\theta''^{(k+1)}+\frac{1}{4}\mathrm{Pr}\,E_n g''^{(k+1)^2}-R_e\,\mathrm{Pr}\,g^{(k+1)}\theta'^{(k+1)}=0, \tag{16}$$

where $g^{(k+1)}$ is known and the derivatives are approximated using the central differences.

By employing central difference discretization on equation (16), we obtain diagonally dominant linear system which permits us to apply SOR method.

4. Results and discussion

In this section, our main concern is to study numerically the flow and heat transfer characteristics of the problem under consideration through graphs and tables. The Reynolds number R_e, the Eckert number E_n, the radiation parameter Rd, the Prandtl number Pr and the porosity parameter ε are the parameters under consideration. The quantities of engineering applications are $g''(\pm 1)$ and $\theta'(\pm 1)$ at disks.

The precise numerical results at the consecutive three grid sizes with their extrapolated values are shown in Table 1. By decreasing the step-size, the numerical results converge. It gives us confidence about our computational procedure. Table 2 demonstrates the influence of viscous dissipation over the heat transfer rate. It is observed that heat transfer rate increases at both the disks by increasing E_n. The shear stress and the heat transfer rate are might be increased by the influence of stretching Reynolds number at both the disks as illustrated in Table 3.

TABLE 1. The extrapolated values of $\theta(\eta)$ for $R_e = 6, Pr = 1.7, E_n = 1.8, Rd = 0.3, \varepsilon = 2$

	$\theta(\eta)$			
η	1st grid η ($h = 0.02$)	2nd grid ($h = 0.01$)	3rd grid ($h = 0.005$)	Extrapolated Values
-0.8	1.677379	1.679468	1.679991	1.680165
-0.4	1.601356	1.603791	1.604401	1.604604
0.0	1.456151	1.458596	1.459208	1.459413
0.4	1.311693	1.314135	1.314746	1.314950
0.8	0.916132	0.918079	0.918567	0.918729

TABLE 2. The effect of viscous dissipation on heat transfer rate with

E_n	$\theta'(-1)$	$\theta'(1)$
0.0	-1.075537	-0.699288
0.2	-0.161460	-1.359030
0.4	0.752616	-2.018773
0.6	1.666691	-2.678516
0.8	2.580768	-3.338259

$R_e = 6, \alpha = 0.8, \Pr = 1.7, \varepsilon = 1.7, Rd = 0.3$

TABLE 3. Shear stress and heat transfer rate for $\alpha = 0.9, E_n = 1.8, \varepsilon = 2, Rd = 0.3, \Pr = 1.7$ with various R_e

R_e	$g''(-1)$	$\theta'(-1)$	$g''(1)$	$\theta'(1)$
0	5.756967	5.628835	-5.556967	-6.213612
1.5	7.218131	6.222288	-6.701043	-6.698050
3	8.469767	6.741306	-7.743222	-7.206725
4.5	9.570051	7.218109	-8.681926	-7.707828
6	10.555272	7.662835	-9.532485	-8.191867

The effects of porosity parameter ε is represented by Table 4. The influence of the porosity parameter of the medium is to increase the wall shear stress in magnitude. Moreover, it has the tendency to enhance the heat transfer rate. Table 5 predicts the effect of the disk stretching α on

shear stress and as well as on the heat transfer rate. When $\alpha = 0,$ we have the asymmetric case. That is shear stress shows opposite trend at both the disks which is minimum at the upper disk and maximum in magnitude at the lower one. It is worth mentioning that as α increases, $g''(1)$ also increases so that for $\alpha = 1,$ the shear stress becomes equal in magnitude at both the disks. The disk stretching parameter gives rise to the heat transfer rate. It is noted that the heat transfer rate decreases by increasing the radiation as represented by Table 6, whereas Table 7 predicts that the increase of Prandtl number is responsible for increasing the heat transfer rate.

TABLE 4. Shear stress and heat transfer rate for $R_e = 6, \alpha = 0.9, E_n = 1.8, Rd = 0.3, \Pr = 1.7$ with various ε

ε	$g''(-1)$	$\theta'(-1)$	$g''(1)$	$\theta'(1)$
1.1	9.312990	7.426621	-8.379696	-8.106124
2.2	10.805049	7.735718	-9.762901	-8.232702
3.3	12.054412	8.187522	-10.910432	-8.518821
4.4	13.144872	8.666353	-11.906887	-8.848893
5.5	14.121779	9.138610	-12.796732	-9.186716

TABLE 5. Shear stress and heat transfer rate for $R_e = 6, E_n = 1.8, \Pr = 1.7, \varepsilon = 2, Rd = 0.3$ with various α

α	$g''(-1)$	$\theta'(-1)$	$g''(1)$	$\theta'(1)$
0.0	9.359471	4.117056	-0.976899	-0.345575
0.3	9.709519	5.192108	-3.473094	-1.556839
0.6	9.994733	6.394298	-6.232626	-4.119971
0.9	10.231352	7.605144	-9.243976	-8.145757
1.0	10.301558	7.990089	-10.301558	-9.814016
1.2	10.431114	8.711306	-12.494610	-13.628531

TABLE 6. Heat transfer rate for $R_e = 6, \alpha = 0.9, E_c = 1.8, \varepsilon = 2, \Pr = 1.7$ with various Rd

Rd	$\theta'(-1)$	$\theta'(1)$
0.0	11.579827	-11.926729
0.1	9.908889	-10.331942
0.2	8.648482	-9.130345
0.3	7.662835	-8.191867
0.4	6.870388	-7.438293

TABLE 7. Heat transfer rate for $R_e = 6, \alpha = 0.9, \varepsilon = 1.7, Rd = 0.3$ with various Pr

Pr	$E_n = 0$		$E_n = 1.6$	
	$\theta'(-1)$	$\theta'(1)$	$\theta'(-1)$	$\theta'(1)$
0.1	-0.523346	-0.516884	-0.078918	-0.893958
0.3	-0.572303	-0.551366	0.779867	-1.699686
0.5	-0.624289	-0.586689	1.662171	-2.530415
0.7	-0.679295	-0.622716	2.569772	-3.387764
0.9	-0.737293	-0.659295	3.504636	-4.273499

Now, the graphical interpretation of our results is given as follows. Figures 1 and 2, represent the respective configuration of the model as well as the streamlines for the flow and heat transfer problem between the two disks.

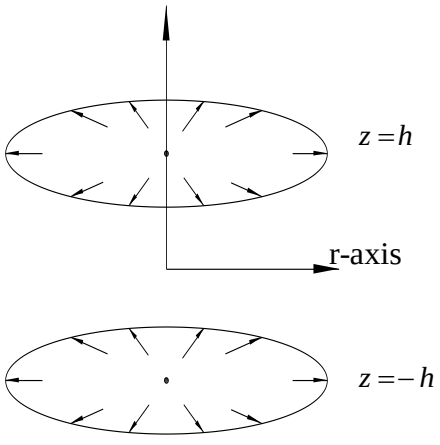

Figure 1. Physical Model

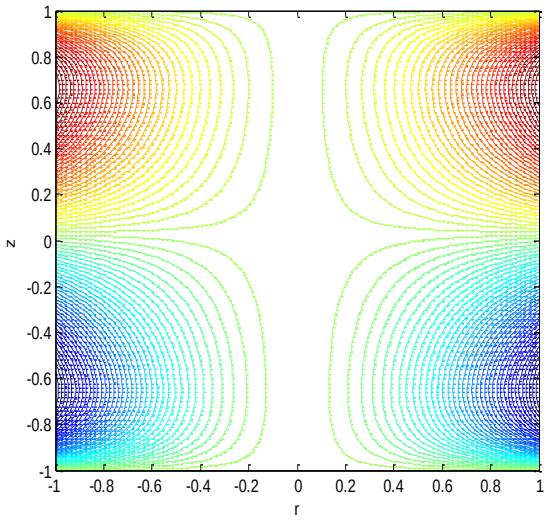

Figure 2. Flow Streamlines for $\alpha = 0.9, E_n = 1.8, \varepsilon = 2, Rd = 0.3, \Pr = 1.7, R_e = 6$

The effects of R_e on axial velocity is shown by Fig. 3. The velocity field decreases in the upper half region and increases in the lower one by increasing R_e. Figure 4 illustrates the variation in radial component of the velocity for various R_e. These profiles are moved towards the surface of the disks. Further, these profiles fall in the central area between the disks. Moreover, the temperature variation for various R_e is represented by Fig. 5. In the starting stage, the effect of the stretching is significant near the lower disk. For $-0.8 \le \eta \le 0.6$, the temperature falls whereas these profiles rise for $\eta > 0.6$.

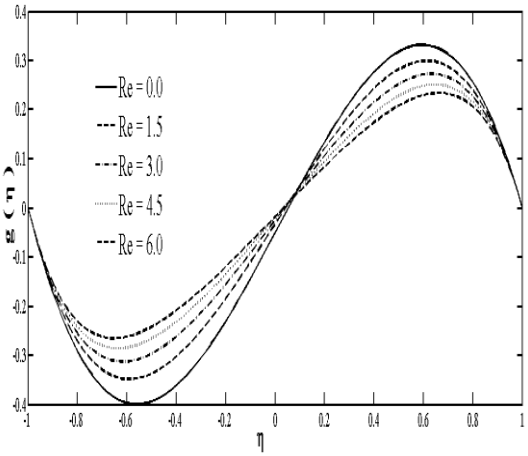

Figure 3. Variation of axial velocity for $\Pr = 1.7, \alpha = 0.9, E_n = 1.8, \varepsilon = 2, Rd = 0.3$ **and various** R_e

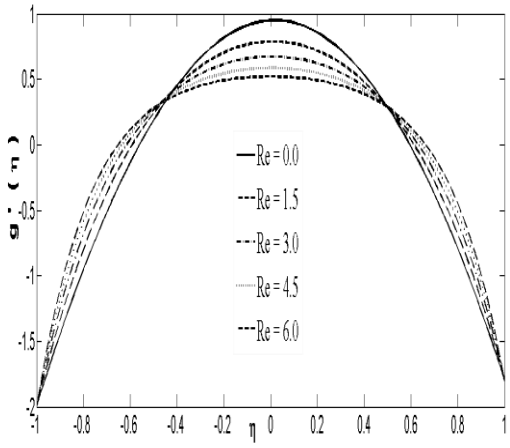

Figure 4. Variation of radial velocity for $\Pr = 1.7, \alpha = 0.9, E_n = 1.8, \varepsilon = 2, Rd = 0.3$ **and various** R_e

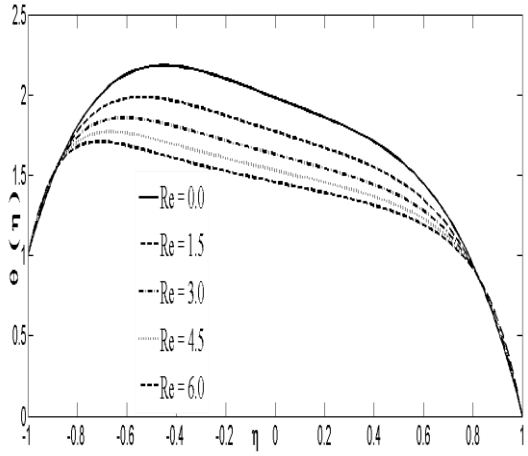

Figure 5. Variation of temperature for $\Pr = 1.7, \alpha = 0.9, E_n = 1.8, \varepsilon = 2, Rd = 0.3$ **and various** R_e

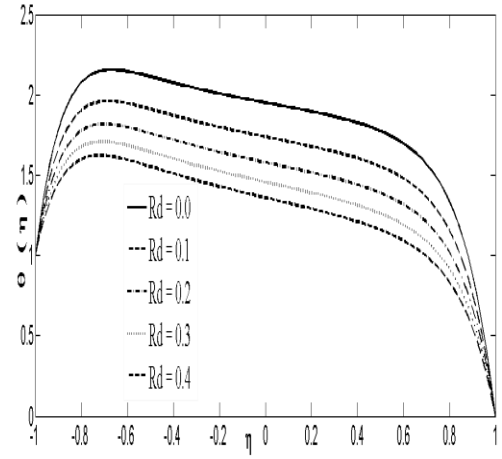

Figure 6. Variation of temperature for $\Pr = 1.7, R_e = 6, \alpha = 0.9, E_n = 1.8, \varepsilon = 2$ **and various** Rd

By Figs. 6 and 7 it is predicted that with the increase in radiation, the temperature profiles fall whereas these profiles rise by the increase of viscous dissipation across the domain respectively. It is noted that near the lower disk, thermal reversal may occur due to increase of Eckert number as shown by Fig.7. The effects of porosity parameter ε on axial velocity are represented by Fig. 8. By increasing ε, axial velocity component decrease in magnitude whereas profiles of the radial velocity component are stretched towards the boundaries. These profiles show falling trend in the central region between the disks as shown in Fig. 9. Physically, the fluid motion is associated to the much resistance which results from the manifestation of the permeable medium due to which a reduction in the velocity and momentum layer thickness occurs. Thus it is referred that the appearance of porous medium plays significant impact in controlling the flow nature. Fig. 10. shows that by increasing the porosity parameter ε, the temperature profiles may decrease.

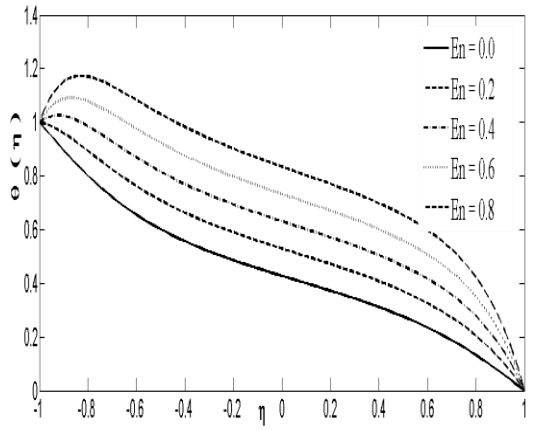

Figure 7. Variation of temperature for $Rd = 0.3, R_e = 6, \alpha = 0.8, \Pr = 1.7, \varepsilon = 1.7$ **and various** E_n

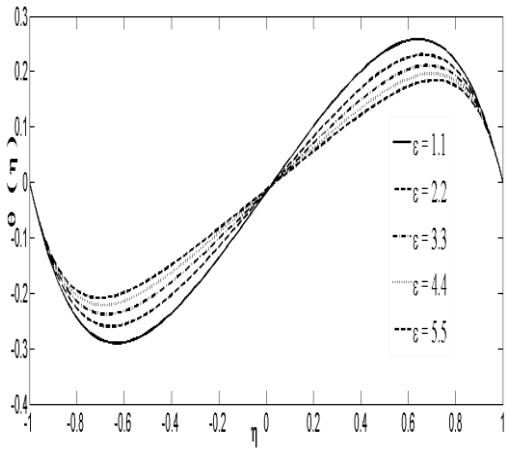

Figure 8. Variation of axial velocity for $\Pr = 1.7, R_e = 6, \alpha = 0.9, E_n = 1.8, Rd = 0.3$ **and various** ε

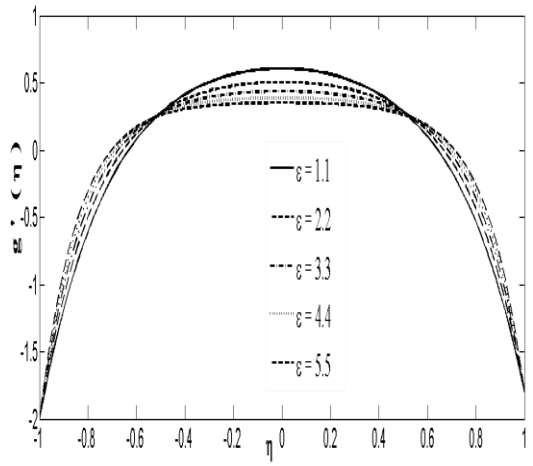

Figure 9. Variation of radial velocity for $\Pr = 1.7, R_e = 6, \alpha = 0.9, E_n = 1.8, Rd = 0.3$ **and various** ε

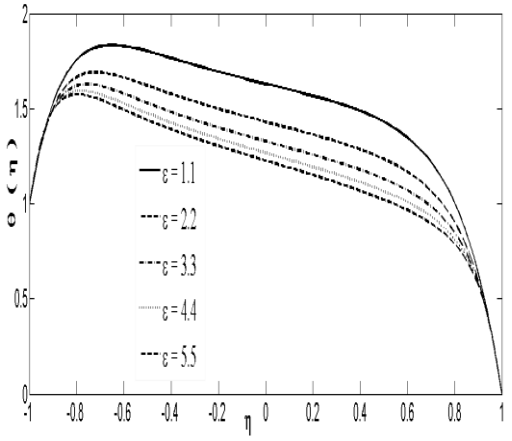

Figure 10. Variation of temperature for $\Pr = 1.7, R_e = 6, \alpha = 0.9, E_n = 1.8, Rd = 0.3$ **and various** ε

From Fig. 11. it is predicted that the temperature increases in the entire domain with the increase in the Prandtl number.

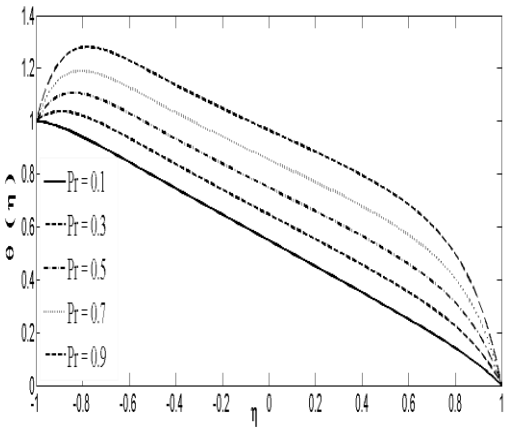

Figure 11 a. Variation of temperature for

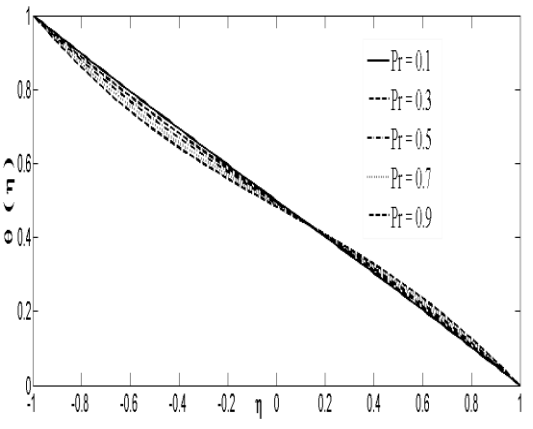

Figure 11 b. Variation of temperature for

$Rd = 0.3, R_e = 6, \alpha = 0.9, E_n = 1.8, \varepsilon = 2$ **and various** Pr	$Rd = 0.3, R_e = 6, \alpha = 0.9, E_n = 0, \varepsilon = 2$ **and various** Pr

Lastly, Figs. 12-14 present the change in behavior of velocities (axial & radial) and temperature under the effect of disk stretching parameter α. It is observed that before $\eta = -0.8$, the influence of α on $f(\eta)$ is not significant. However, for $\eta > -0.8$, it becomes more influential and in the whole domain, these profiles rise as it may be noted in Fig. 12. The velocity component $f'(\eta)$ increases with α across a major portion of the area near the lower disk. While for $\eta > 0.4$, the trend is reversed near the upper one as shown in Fig. 13. The radial velocity tends to be symmetric and parabolic. Fig. 14 illustrates that the temperature gradient is enhanced in the entire domain by increasing the disk stretching parameter whereas the temperature decreases by increasing η.

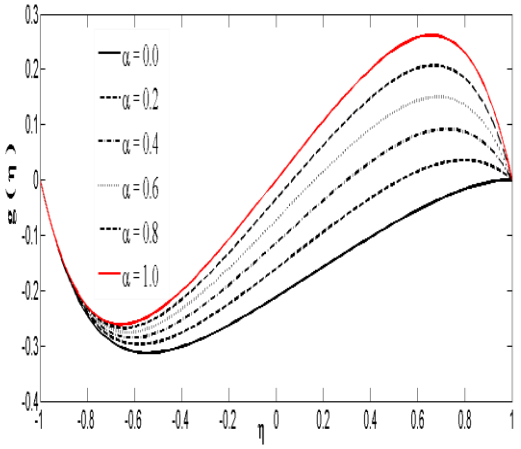

Figure 12. Variation of axial velocity for $Rd = 0.3, R_e = 6, E_n = 1.8, \Pr = 1.7, \varepsilon = 2$ **and various** α

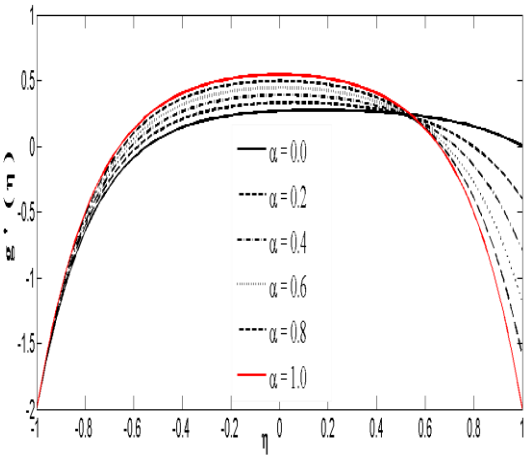

Figure 13. Variation of radial velocity for $Rd = 0.3, R_e = 6, E_n = 1.8, \Pr = 1.7, \varepsilon = 2$ **and various** α

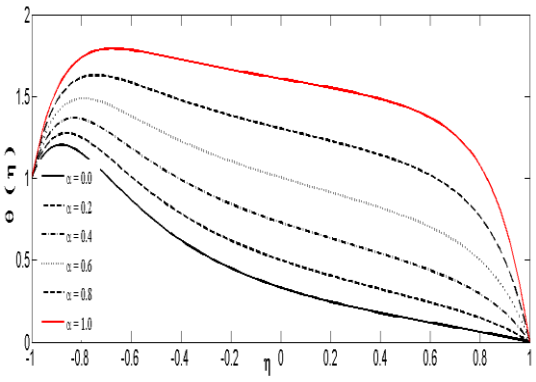

Figure 14. Variation of temperature for $Rd = 0.3, R_e = 6, E_n = 1.8, \Pr = 1.7, \varepsilon = 2$ **and various** α

CONCLUSIONS

A comprehensive study is presented for the disk stretching, viscous dissipation and radiation using an approximation method based on Quasi linearization and finite difference discretization. The following results have obtained.

- The physical quantities such as shear stress as well as the heat transfer rate are enhanced by increasing the porosity parameter $1.1 \le \varepsilon \le 5.5$.
- Near the lower disk, the thermal reversal is occurred due to strong viscous dissipation, and by increasing the $E_n, 0.0 \le E_n \le 0.8,$ temperature decreases away from the lower disk.
- Due to the effects of radiation number $0.0 \le Rd \le 0.4,$ the Nusselt number is decreased over the disks.
- An enhancement of temperature gradient occurs due to increase in the disk stretching parameter $0 \le \alpha \le 1$.

Nomenclature

c_p	- the specific heat capacity, $\left[jkg^{-1}K^{-1} \right]$	Greek Symbols	
p	- the fluid pressure, $\left[Nm^{-2} \right]$	σ	- Stefan-Boltzmann constant, $\left[Wm^{-2}K^{-4} \right]$
q_r	- radiative heat flux, $\left[Wm^{-2} \right]$	k^*	- mean absorption coefficient, $[-]$
T	- the fluid temperature, $[K]$	α	- relative disk stretching parameter, $(=S_2/S_1)$, $[-]$
$u, v \& w$	- velocity components in the radial, transverse and axial directions Respectively, $\left[ms^{-1} \right]$	ε	- porosity parameter, $\left(= h^2/k^{\bullet}\right)$, $[-]$
$S_2 \& S_1$	- stretching strengths of the upper and lower disks respectively, $\left[Nt^{-1} \right]$	η	- the similarity variable, $[-]$
R_e	- stretching Reynolds number, $\left(= \rho S_1 h^2/\mu\right)$, $[-]$	$k^{\bullet}$	- the Darcy permeability, $\left[m^2 \right]$
Pr	- Prandtl number, $\left(= \mu c_p/k_{\circ}\right)$, $[-]$	ρ	- the fluid density, $\left[kgm^{-3} \right]$
E_n	-Eckert number, $\left[= r^2 {S_1}^2/c_p\left(T_1 - T_2\right)\right]$, $[-]$	μ	- the dynamic viscosity, $\left[Nsm^{-2} \right]$

References

[1] Masoud, Z., Faezeh, M., and Mohammad, R. S., Experimental Investigation of the Permeability and Inertial Effect on Fluid Flow Through Homogeneous Porous Media, *Irranian Journal of Chemistry and Chemical Engineering*, *27* (2008), 2, pp. 33-38

[2] Mónica, S. N. O., Manuel, A. A., Fernando, T. P., and Gareth, H. M., Newtonian Fluid Flow Through Microfabricated Hyperbolic Contractions, *Experiments in Fluids, 43* (2007), 2-3, pp. 437–451

[3] Hamza, E. A., A Similar Flow Between two Disks in the Presence of a Magnetic Field, *Journal of Applied Fluid Mechanics, 56* (2009), 1, pp. 218-221

[4] Milan, B., Steady Flow of Incompressible Fluid Between two Co-Rotating Disks, *Applied Mathematical Modelling*, 35 (2011), 10, pp. 5225-5233

[5] Y, L. Y., Yee-Kwong L., and Ash K., Slow Steady Viscous Flow of Newtonian Fluids in Parallel-Disk Viscometer with Wall Slip, *Journal of Applied Mechanics, 75* (2008), 4, pp. 041001

[6] Lynn, O. W., et al., Flow Between a Stationary and a Rotating Disk with Suction, *Journal of Fluid Mechanics, 85* (2006), 3, pp. 479-496
[7] Zweig, J. E., et al., Two-Fluid Flow Between Rotating Annular Disks, ASME *Journal of Lubrication Technology, 98* (2010), 2, pp. 214-222
[8] Qayyum, A., Awais, M., Alsaedi, A., and Hayat, T., Unsteady Squeezing Flow of Jeffery Fluid Between two Parallel Disks, *Chinese Physical Society and IOP Publishing Ltd, 29* (2012), 3, pp. 034701. doi:10.1088/0256-307x/29/3/034701
[9] Shalini, J., et al., Radiation Effects in Flow Through Porous Medium over a Rotating Disk with Variable Fluid Properties, *Advances in Mathematical Physics, 2016* (2016), pp. 9671513
[10] Wijaya, I., et al., Simulation of Fluid Flow and Heat Transfer in Porous Medium Using Lattice Boltzmann Method, *Journal of Physics, 877* (2017), pp. 012056
[11] Hussain, M. F., Numerical Analysis of Nanofluids with Convective Heat Transfer Through Porous Disks, *Caspian Journal of Computational and Mathematical Engineering , 2* (2017), pp. 2476– 5252
[12] Nandeppanavar, M. M., et al., Effect of Viscous Dissipation and Thermal Radiation on Heat Transfer over a Non-Linearly Stretching Sheet Through Porous Medium, *International Journal of Applied Mechanics and Engineering, 18* (2013), 2, pp. 461-474
[13] Srinivasacharya D., et al., Chemical Reaction and Radiation Effects on Mixed Convection Heat and Mass Transfer over a Vertical Plate in Power-Law Fluid Saturated Porous Medium , *Journal of the Egyptian Mathematical Society, 24* (2016), 1, pp. 108-115
[14] Hobiny, A., Ahmad, B., Alsaedi, A., Jalil, M., and Asghar, S., Similarity Solution for Flow over an Unsteady Nonlinearly Stretching Rotating Disk, *AIP Advances, 5* (2015), 4, pp. 047113
[15] Sreenivasulu, P., Poornima, T., and Reddy, N. B., Thermal Radiation Effects on MHD Boundary Layer Slip Flow Past a Permeable Exponential Stretching Sheet in the Presence of Joule Heating and Viscous Dissipation, *Journal of Applied Fluid Mechanics, 9* (2016), 1, pp. 267-278
[16] Rashidi, M. M., Pour, S. A. M., Hayat, T., and Obaidat, S., Analytic Approximate Solutions for Steady Flow over a Rotating Disk in Porous Medium with Heat Transfer by Homotopy Analysis Method, *Computers & Fluids, 54* (2012), pp.1–9
[17] Rabhi., Amami, B., Dhahri H., and Mhimid A., Heat Transfer and Entropy Generation in Porous Microduct with Slip Boundary Condition Using Lattice Boltzmann Method Under Nonequilibrium Conditions, *Journal of Porous Media, 20* (2017), 3, pp. 227-247
[18] Xu, H., Zhao, C., and Vafai, K., Analytical Study of Flow and Heat Transfer in an Annular Porous Medium Subject to Asymmetrical Heat Fluxes, *Heat and Mass Transfer, 53* (2017), 8, pp. 2663-2676
[19] Turkyilmazoglu, M., Flow and Heat Simultaneously Induced by two Stretchable Rotating Disks, *Physics of Fluids, 28* (2016), 4, pp. 10.1063/1.4945651
[20] Eringen, A. C., Theory of Micropolar Continua In. *Proceedings of the Ninth Midwestern Conference,* 1965
[21] Eringen, A. C., Simple Micro Fluids, *International Journal of Engineering Science, 2 (*1964), pp. 205-217